Asian Journal of Chemistry; Vol. 37, No. 7 (2025), 1785-1795

ASIAN JOURNAL OF CHEMISTRY

https://doi.org/10.14233/ajchem.2025.33980

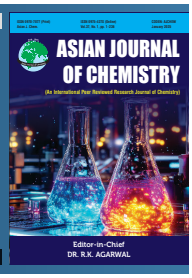

Synthesis, Characterization and Anticancer Potency of Copper(II) Complex of Coumarin and 4-(2-Aminoethyl)morpholine based Schiff Base

NEETA SINGH[1,2], ANAND KUMAR YADAV[1,2], MANOJ SILWAL[3], SABITA SHRESTHA[2] and PARAS NATH YADAV[2,*]

[1]Department of Chemistry, Patan Multiple Campus, Tribhuvan University, Kathmandu, Nepal
[2]Central Department of Chemistry, Tribhuvan University, Kathmandu, Nepal
[3]New Horizon English Boarding School, Rupendehi, Butwal, Nepal

*Corresponding author: E-mail: pnyadav219@gmail.com

Received: 2 May 2025; *Accepted*: 26 June 2025; *Published online*: 30 June 2025; AJC-22055

A Schiff base ligand (L) synthesized from coumarin and 4-(2-aminoethyl)morpholine and its copper(II) complex was synthesized and characterized by elemental analysis, HRMS, UV-Vis, FT-IR, NMR and EPR spectroscopy. The IR band at 3358 cm^{-1} correspond to the O-H stretching vibration in the free ligand was intact and shifted to 3336 cm^{-1} in the complex. In ^1H NMR, aromatic protons of the ligand were observed at 7.96-7.26 ppm while that of morpholine and ethylene were observed at 3.71-2.63 ppm, conforming the formation of Schiff base. Similarly, ^{13}C NMR exhibited the peaks related to the individual carbon atoms in the ligand. Formation of the proposed ligand and complex was additionally supported by the HRMS spectra. Further, molecular structure of the ligand (L) was confirmed by X-ray crystallography having orthorhombic space group $P2_12_12_1$. The unit cell dimensions were a = 5.4258(3) Å, b = 12.4715(9) Å, c = 23.6349(16) Å. The observed g values, $g_{\parallel} > g_{\perp} > g_e$ ($g_{\parallel}$; 2.3559 and $g_{\perp}$; 2.0669) for the complex indicated the Cu(II) ion in the square planner geometry. The anticancer potency of the compounds was performed with the MCF-7 cell line. The IC_{50} values of the free ligand was found 256.60 ± 0.11 µg/mL and that of complex [$CuLCl_2$], 118.50 ± 0.40 µg/mL. Cell cycle study of [$CuLCl_2$] complex showed a higher proportion of cells in G1 (33.18%) and S (23.40%) phases and a lower proportion of cells in G2 phase (30.91%). A molecular docking study showed binding affinity of the ligand; ΔG = -7.3 kcal/mol and it's complex with ΔG = -8.0 kcal/mol along with H-bond interaction with protein EGFR, which indicates potential interactions with the biological targets.

Keywords: Anticancer potency, Coumarin, Molecular docking, Morpholine, Schiff base.

INTRODUCTION

Cancer is characterized by the uncontrolled growth of abnormal cells in the body. Normally, old cells die, but in cancer, it multiplies rapidly, producing abnormal cells that disrupt normal DNA replication and interfere with protein secretion in the healthy cells. Common types of cancer, such as prostate, cervical, lung and breast cancer, are spreading widely around the world [1]. Cancer is the second leading cause of death worldwide, after cardiovascular diseases. Despite advancements in chemotherapy, many patients do not respond successfully, often due to multidrug resistance or side effects. This underscores the critical need for ongoing research into new anticancer compounds that are both more effective and have fewer adverse effects [2].

Coumarin and its derivatives are a prominent class of organic heterocycle having widespread application across diverse biological, chemical and physical fields. Naturally occurring coumarins are abundant in many plants, especially in high concentrations in tonka beans, apricots, lavender, sweet clover, cherries, cinnamon and strawberries [3]. Coumarin can interact noncovalently with multiple biological targets through mechanisms such as metal coordination, hydrogen bonding and π-π interactions. Due to these properties, coumarin has been widely used in drug development, demonstrating significant pharmacological effects against malaria, fungal & bacterial infections and cancer [4]. Both natural and synthetic coumarins display cytotoxic effects through diverse mechanisms, driven by their unique structural features to suppress the proliferation of cancerous cells. These include inhibition of down-regulating oncogene

expression, telomerase enzyme, induction of caspase-9-mediated apoptosis, protein kinase activity, cell cycle arrest in the G2/M, G0/G1 phase and have an impact on the P-glycoprotein of the cancer cell [5]. Hydroxy derivatives of coumarins, such as 7-hydroxycoumarins and 4-hydroxycoumarins, exhibited a wide range of physiological and pharmacological activities and are commonly utilized in the synthesis of various coumarin derivatives [6]. Coumarin derivatives have also demonstrated significant pharmacological effects *e.g.* antibacterial, anti-inflammatory, antioxidant, antidiabetic, anticoagulant, neuroprotection, anticonvulsant and anticancer [7,8]. Some coumarins and their active metabolite have shown sulfatase and aromatase inhibitory activities. Although most of the natural coumarins exhibited hepatotoxicity, some of its derivatives are in clinical trial, which may be a new therapeutic agent [9].

A large number of biological activities are known to depend critically on the transition metal ions and reactive oxygen species. Copper(II) ions, in the human body, are crucial for signal transduction, osteogenesis, neuromodulation and cellular oxygen activation [10]. Schiff bases play a key role in the development of bioactive compounds due to their diverse pharmacological properties. Schiff bases and their metal complexes are valued for their anti-inflammatory, antifungal, antibacterial, antiviral and anticancer activities, highlighting their potential in therapeutic applications [11]. The anticancer efficacy increases when complexation occurs with the metal ions like Cu(II) ion [12-14].

Morpholine-based Schiff bases demonstrate exceptional stability in biological environments, making them particularly well-suited for long-term applications, especially in DNA modification. Such deliberations are essential for the progression of ligands with morpholine moiety and their associated metal complexes for prospective uses as anticancer agent [15]. It is also acknowledged that the presence of metal ions bonded to the biologically active compounds make them more effective in various types of biological activities [16]. In this work, we have synthesized coumarin aminoethyl morpholine Schiff base and its Cu(II) complex. The cytotoxicity of the synthesized compounds was evaluated *in vitro* against the MCF-7 cell line and molecular docking was performed with the EGFR protein. The molecular structure of the ligand (L) was confirmed through the single-crystal X-ray crystallography.

EXPERIMENTAL

4-Hydroxycoumarin, 4-(2-aminoethyl)morpholine (Alfa Aesar), piperdine (Himedia), pyridine (Merck), acetyl chloride (Fisher Scientific) and hydrochloric acid (Fisher Scientific), trypsin-EDTA (Gibco), penicillin-streptomycin (Sigma- Aldrich), DMEM (Himedia), MTT, DMSO and ethanol (Genetix Biotec Pvt. Ltd) were used as received.

FT-IR spectra were recorded using SHIMADZU Tracer 100 instrument in wave number range of 4000–500 cm^{-1}. UV-Vis spectra of the compounds (5×10^{-5} M, DMSO solution) using Agilent technologies cary 60 UV-Vis spectrophotometer, carried out in the range of 200-800 nm. UV-Visible spectra of the solid-state compounds were measured using the instrument UV-2600i (A12596080171ML (model), 2.0 nm (slit width), external (2 detectors), 323 nm (light source switch wavelength), 830 nm (detector switch wavelength). The FTIR and UV-Vis data were processed with Origin-pro software. Melting points were determined on Philip Harris melting point apparatus. The elemental analysis (CHN) was done using the LECO Truspec Micro analyzer, high resolution electron spray ionization mass spectra were recorded using LC-QTOF-HRMS spectrometer, XRD (Bruker D8 Venture SC) Mo/$K\alpha$ radiation) and EPR (JES-FA200 ESR spectrometer with X-band) were measured. NMR spectra (BRUKER bio spin GmbH NMR spectrometer, 400 MHz) was recorded in DMSO-d_6 by using TMS as internal standard. Chloride content in the copper(II) complex was determined by potentiometric method [17].

Acetylation of hydroxycoumarin: 4-Hydroxycoumarin (6.16 g, 0.038 mol) in dry pyridine (48 mL) and catalytic amount of piperidine (0.1 mL) was cooled to 0-5 ºC. Then acetyl chloride (4.34 g, 0.056 mol) was added dropwise and the mixture was stirred for 48 h at 20 ºC. Then solution was poured into ice-cold water (140 mL) and the product was obtained by maintaining pH 1-2 by using 2 M HCl. The precipitate formed, was filtered by suction, washed with water until neutral and dried at 40 ºC (**Scheme-I**). The compound was recrystallized in ethanol/water (1:1); m.p.: 138 ºC (lit. [18], 134-136 ºC. Purity of the compounds was checked by TLC.

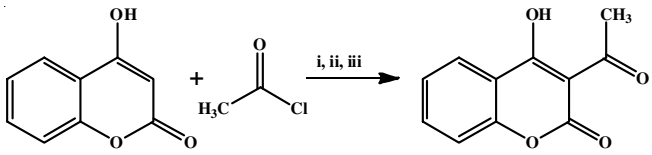

Scheme-I: Acetylation of 4-hydroxycoumarin; (i) pyridine (ii) piperidine (iii) stir, R.T., 48 h

Synthesis of coumarin Schiff base (L): The equimolar mixture of 3-acetyl-4-hydroxycoumarin (1 mmol, 0.204 g) and 4-(2-aminoethyl)morpholine (1 mmol, 0.130 g) in absolute ethanol (20 mL) with 2-3 drops of glacial acetic acid was refluxed at 80 ºC for 6 h. Then, the obtained solid was allowed to cool at room temperature, washed with absolute alcohol, recrystallized from ethanol and dried at 40-45 ºC overnight (**Scheme-II**) [16]. The purity of the product was checked by TLC.

(*E*)-4-Hydroxy-3-(1-((2-morpholinoethyl)imino)ethyl)-2*H*-chromen-2-one (L): Yield: 87%; colour: pinkish white;

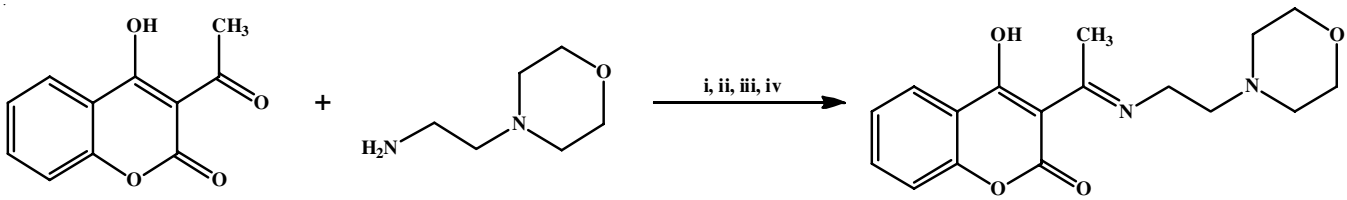

Scheme-II: Synthesis of Schiff's base; (i) EtOH, (ii) AcOH, (iii) reflux, (iv) 80 ºC, 6 h

m.p.: 106 ºC. Elemental analysis of $C_{17}H_{20}N_2O_4$, Calcd. (found) %: C, 64.54 (64.49); H, 6.37 (6.31); N, 8.86 (8.79); FTIR (KBr, ν_{max}, cm^{-1}); 3358 (b, OH), 2980, 2845, 2792 (C-H), 1678 (s, C=O, lactone), 1615 (s, C=N); 1467, 1409 (C=C); 1231 (C-O); ^{1}H NMR (400 MHz, DMSO-d_6), δ ppm: 13.62 (s, 1H, OH); 7.96 (dd, *J* = 1.6 Hz, HC5); 7.62 (dd, *J* = 1.6 Hz, HC6), 7.26 (m, HC8, HC7), 3.71, 3.63 (t, morpholine); 2.67, 2.64 (t, CH_2-CH_2), 2.63 (s, CH_3); ^{13}C NMR (DMSO-d_6), δ ppm: 179.29 (C=N), 175.64 (C4), 162.10 (C2), 153.00 (C10), 133.88 (C7), 125.71 (C5), 123.59 (C6), 120.35 (C9), 116.19 (C8), 96.04 (C3), 66.24, 55.54 (CH_2-CH_2) 52.89, 40.92 (morpholine), 18.71 (CH_3); UV-Vis (DMSO, λ_{max}, nm) 250 sh (π-π*), 320 br (n-π*), Powder; 238 br, 299 br (π-π*), 352 br (n-π*); HR-ESI MS (*m/z*) $[M+H]^+$ found (calcd.); 317.1556 (317.1496).

Synthesis of copper(II) complexes of Schiff base; [CuLCl$_2$]: Copper(II) complex was prepared by refluxing equimolar mixture of $CuCl_2{\cdot}2H_2O$ (0.170 g, 1 mmol) in 10 mL ethanol and Schiff base (1 mmol, 0.316 g) in 15 mL ethanol for 3 h, as shown in **Scheme-III**. The resulting precipitate was filtered, washed with 1:1 (v/v) EtOH:H_2O, followed by diethyl ether [16]. It was dried at 40 ºC overnight and then at 80 ºC for 1 h.

(*E*)-4-Hydroxy-3-(1-((2-morpholinoethyl)imino)ethyl)-2*H*-chromen-2-one Cu(II)chloride; [CuLCl$_2$], Yield: 45%; colour: greenish blue; m.p.: 272 ºC; Elemental analysis of $C_{17}H_{20}N_2O_4Cl_2Cu$; calcd. (found) %; C, 45.29 (45.21); H, 4.47 (4.39); N, 6.21 (6.11), Cl, 15.73 (15.64); FTIR (KBr, ν_{max}, cm^{-1}): 3336 (b, OH), 2964, 2924, 2852 (C-H), 1667 (s, C=O, lactone), 1597 (s, C=N), 1463, 1413 (C=C), 1221 (C-O); UV-Vis (DMSO, λ_{max}, nm), 253 sh (π-π*), 320 br (n-π*), powder; 240br, 301 br, 345 sh (π-π*), 414br (n-π*); HR-ESI MS (*m/z*) $[M+H]^+$ found (calcd.); 450.2918 (450.0169).

Anticancer screening

MTT assay: Cytotoxicity of the compounds on MCF-7 (Procured from NCCS, Pune) cell line was determined by MTT Assay. The cells (10000 cells/well) were cultured in 96 well plate for 24 h in DMEM medium supplemented with 10% FBS and 1% antibiotic solution at 37 ºC with 5% CO_2. Cells without treatment were considered as control and cells without MTT were considered as blank. After incubation for 24 h, MTT solution (a final concentration of 250 µg/mL) was added to cell culture and further incubated for 2 h. At the end of the experiment, the culture supernatant was removed and cell layer matrix was dissolved in 100 µL DMSO and read in an Elisa plate reader (iMark, Biorad, USA) at 540 nm [19,20]. IC_{50} was calculated by using software Graph Pad Prism 6. Images were captured under an inverted microscope (Olympus ek2) using Camera (AmScope digital camera 10 MP Aptima CMOS). 50% inhibitory concentration (IC_{50}) was presented as Mean ± SEM (standard error of mean). It was calculated by using the following formula:

$$\text{Viable cells (\%)} = \frac{A_{test}}{A_{control}} \times 100$$

where A_{test} = absorbance of test sample, $A_{control}$ = absorbance of control.

Cell cycle analysis with flow cytometer-MCF-7: Cells were plated and treated with the samples for 24 h. Cells without treatment were considered as control. After incubation period, cells were harvested using the trypsin and collected in 1.5 mL tube and washed once with 500 µL chilled PBS. Approximately 10^6 cells were suspended in 100 µL of PBS and vortexed gently to obtain a mono-dispersed cell suspension, with minimal cell aggregation. Cells were then fixed by transferring this suspension, with a pipette, into centrifuge tubes containing 900 µL of 70% ethanol, on ice and incubated for at least 2 h at 4 ºC. Cells may be stored in 70% ethanol at 4 ºC for weeks. After fixation, cell was centrifuged and pellet was suspended in 500 µL of propidium iodide (PI) staining solution (0.1% (v/v) Triton X-100, 10 µg/mL PI and 100 µg/mL DNase-free RNaseA in PBS) and kept in dark at room temperature for 30 min, at 37 ºC for 10 min. Then the compounds were acquired on a flow cytometer.

Flow cytometry cell cycle analysis (MCF7) of [CuLCl$_2$]: The treatment induced significant changes in the cell cycle distribution of the sample. Compared to the control group (24.87% in G1, 15.27% in S and 34.44 % in G2) and in the treated group [$CuLCl_2$] showed a higher proportion of cells in G1 (33.18%) and S (23.40%) phases and a lower proportion of cells in G2 phase (30.91%) [21,22].

Copper complexes usually exhibit more cytotoxic potency than the corresponding free ligand, because of development of new mechanisms of action after the coordination, like; redox activity, DNA binding that leads to cell death, interaction with biological targets, readily donate or accept electrons (redox property), generation of reactive oxygen species (ROS) that can promote apoptosis, increased lipophilicity that enhance up take by cells, specific property of complex for binding with the biological targets [11].

Schiff base of 2-hydroxyacetophenone with 4-(2-aminoethyl)morpholine and its Cu(II) complex were tested for their cell's viabilities in MCF-7 cells. The ligand did not show significant activities even at higher concentration, while Cu(II) complexes exhibited the MCF-7 cells growth in a dose-dependent

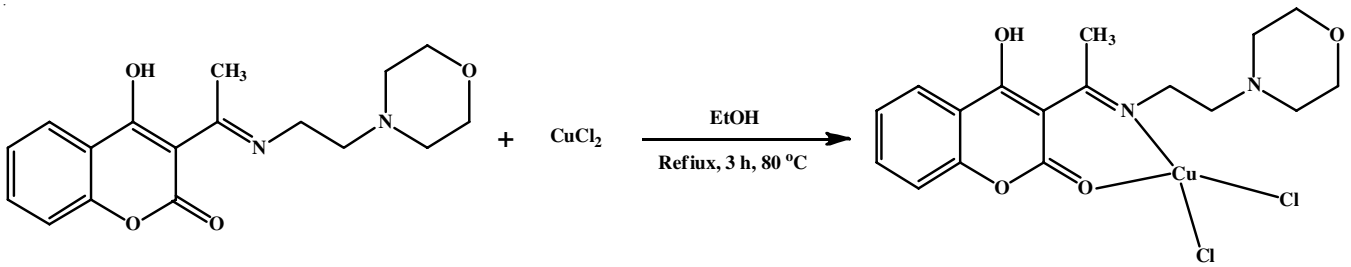

Scheme-III: Synthesis of copper complexes of Schiff's base; [$CuLCl_2$]

manner with EC_{50} (μg/mL) 37.58 and 4.25 for [CuLCl] and [CuLBr] complexes, respectively [16]. Cobalt(III) complex of Schiff base from 2-acetylpyridine and 4-(2 aminoethyl)-morpholine showed significant growth inhibition in MCF-7 cell line. The compound could induce apoptosis by alteration of nucleus morphology and mitochondrial membrane changes, inhibition of colony formation, DNA fragmentation and cytopathologic effects [23].

In silico studies of ligand and its copper complex

Pharmacokinetics study: The drug-like characteristics of the synthesized Schiff base ligand L and its copper complex [$CuLCl_2$] was identified using the available bioinformatics technology, swissADME http://www.swissadme.ch/ [4] and the toxicity class was predicted using the ProTox-3.0 server https://tox.charite.de/protox3/ [25]. Moreover, pkCSM https://biosig.lab.uq.edu.au/pkcsm/prediction was used to perform the absorption, distribution, metabolism, excretion and toxicity (ADMET) study [26].

Binding site prediction: The binding sites of the co-crystallized ligand was predicted using their binding pockets, which were verified by a comprehensive review of the literature [27].

Preparation of ligand structures: 2D structures of the synthesized ligand and complex, [$CuLCl_2$] were drawn in ChemDraw and converted to 3D structure utilizing Avogadro software https://avogadro.cc/ and the structures were saved in the .pdb format in BIOVIA Discovery studio. Then the structures were saved in the .pdbqt format after energy minimization in AutoDock Tools (https://vina.scripps.edu/).

Preparation of receptor: The EGFR (L858R, T790M, V948R) crystal structure in complex with 1-{(3R,4R)-3-[5-chloro-2-(1-methyl-1*H*-pyrazol-4-ylamino)-7*H*-pyrrolo[2,3-*d*]-pyrimidin-4-yloxymethyl]-4-methoxy-pyrrolidin-1-yl}-propanone (PF-06459988) (PDB ID: 5HG7) was fetched from the RCSB protein database https://www.rcsb.org/. To build the EGFR protein, all chains and crystalline structures other than the target protein were separated from the retrieved structure and saved in the .pdb format using BIOVIA Discovery Studio software (https://www.3ds.com/products/biovia/discovery-studio). The structure was saved in the pdbqt format after being optimized with Kollmann charges and adding polar hydrogen in the AutoDock tools [28]. The Grid box was designed with the binding site residues where ligand would bind in the center and measured 40 Å × 40 Å × 40 Å enclosing catalytic residues.

Molecular docking experiment: The computational approach is used to predict the binding mechanism and affinity of a ligand to a protein with a 3D structure. Utilizing Auto Dock Tools version 1.5.7, the generated ligand was docked into the binding sites of the EGFR protein. A maximum of nine ligand poses with binding energy (ΔG) in kcal/mol are permitted in the binding pocket of the target protein under AutoDock Vina's standard configuration. The BIOVIA Discovery Studio Visualizer was used to analyze the binding interactions between ligand and EGFR. The most stable binding complex was determined by comparing the hydrogen bond interactions and binding energies between the ligand and catalytic residues that allows to assess the optimal docking poses. The docking strategy was tested using the co-crystallized ligand found in the recovered receptor; a binding pocket was considered acceptable if the RMSD value between the co-crystallized and docked ligands was less than 2 Å.

RESULTS AND DISCUSSION

FT-IR spectroscopy: The IR bands at 3358 cm^{-1} was observed and assigned to the O-H stretching vibration in the free ligand. The absorption bands of the free ligand were observed at 1678 cm^{-1} and 1615 cm^{-1}, which have been attributed to ν(C=O) and ν(C=N) respectively. Stretching vibration of (C-H) was observed at 2980, 2845 and 2792 cm^{-1} in the free ligand. Stretching vibration of (C-O) was observed at 1231 cm^{-1} in free ligands and shifted to 1221 cm^{-1} in the complex. Bands of the coumarin ring (C=C) was observed at 1467, 1409 cm^{-1} in free ligand and shifted to 1463, 1413 cm^{-1} in the complex [29]. When the IR spectra of the copper complex was compared to the spectra of the free ligand, the peak corresponding to the (C=O) stretching of coumarin (1678 cm^{-1}) was shifted to lower wavenumber (1667 cm^{-1}), suggesting its coordination to Cu(II). The ν(C=N) signal observed at 1615 cm^{-1} in the spectra of free ligand shifted to 1597 cm^{-1} in the spectra of complex as complexation decreases the double bond character indicating coordination of the azomethine nitrogen [30]. Thus, the aforementioned facts suggested that the O and N donor atoms from the free ligand coordinated to Cu(II), reduced the electron density in azomethine and lactone oxygen which shifted the C=N and C=O stretch to the lower wave number [31]. Other coordination sites were occupied by the chloride ions in the distorted square planar geometry of the copper complex [32]. Weak stretching vibration of hydrocarbon functionality, C-H appeared at 2980, 2845 and 2792 cm^{-1} are shifted after coordination with Cu(II) ion. The reduction in intensity of the C-H is due to a decrease in the dipole moment. Schiff base ligand interacts with metal ions through specific atoms, confirming coordination, induced changes in electron density and vibrational frequencies [33].

NMR spectroscopy: ^{1}H NMR spectrum of Schiff base ligand exhibited a singlet at 13.62 ppm, attributed to the OH proton. At comparatively more downfield, 13.62 ppm, could be due to the strong intermolecular hydrogen bonding [34]. All the aromatic protons of the free ligand were observed as multiplate at 7.96-7.26 ppm [35]. The ^{1}H NMR shifts showed the various influences on the proton shielding constants within the structure of compound. Morpholine CH_2 was observed at 3.71 and 3.63 ppm. The ethylene protons were observed at 2.67 and 2.64 ppm and methyl peak of the ligand appeared at 2.63 ppm [16]. The electron-withdrawing effect of the acetyl group and the oxygen atom's electronegativity in the coumarin ring significantly impact the chemical shift of protons on the neighbouring carbon causes deshielding of the proton, reducing electron density and resulting in a downfield chemical shift [33].

The ^{13}C NMR spectra of the ligand exhibited the characteristic peak of (C=N) and (C=O) at 179.29 and 162.10 ppm, respectively. The peaks of C4 having -OH substitution appeared at 175.64 ppm [34]. The carbon atoms of the aromatic ring showed the chemical shift at 153.00-116.19 ppm [31]. The

signals of the ethylene carbons were found at 66.24 and 55.54 ppm. The signals of the aliphatic carbons in morpholine ring were observed at 52.89 and 40.92 ppm [16] and signal of the methyl carbon appeared at 18.71 ppm. In the synthesized Schiff base, the peaks are highly influenced due to the adjacent electronegative atoms. The oxygen in the pyrone ring causes a downfield shift for all carbons within the heterocyclic ring, reflecting the deshielding effect [33]. The chemical shift values of all the protons and carbons were seen in the region as expected for the proposed structure.

ESI-HRMS spectrometry: The mass spectrometry data of the ligand and its Cu(II) complex were in good agreement with the calculated value of the proposed molecular structure. The mass spectra were determined in positive mode of HR-ESI-MS spectrometry. The molecular ion peak for the free ligand was due to the $[M+H]^+$ molecular fragment, *m/z*: found (calcd.); 317.1556 (317.1496) and for its copper complex at 450.2918 (450.0169) [35]. HR-ESI produces molecular ions with limited fragmentation and a prominent single peak of $[M+H]^+$ ion is obtained. In the optimized conditions, these spectra produce exact mass of the molecular ion [30]. Thus, the mass spectral data of the Schiff base and its complex agree well with those of the calculated value.

UV-Vis spectroscopy: Electronic spectra of the Schiff base and its Cu(II) complex in DMSO and in powder form, were recorded in the 200-800 nm region. The UV-Vis spectral data of the ligand in DMSO (5×10^{-5} M) showed a strong $\pi \rightarrow \pi^*$ absorption band at 250 nm and in the powder form at 238 and 299 nm [16]. The peaks observed at 320 nm in solution and at 352 nm in powder can be attributed to $n \rightarrow \pi^*$ intra-ligand electronic transitions, which are mostly caused by the azomethine (C=N) of the Schiff base moiety and the carbonyl group (C=O) of the coumarin moiety. The electronic spectra of the Cu(II) complex due to $n \rightarrow \pi^*$ electronic transitions of C=N and C=O chromophores, in powder form showed a bathochromic shift at 414 nm in the complex which is due to the delocalization of the electronic charge within the chelate ring and thereby stabilizing the complex formed [36]. In the powder spectra, peak at 414 nm also include the ligand charge transfer [37]. Due to poor crystal field splitting energy of the ligand, a definite *d-d* transition band was not seen in the UV-Vis spectra of the complex in solution, but it was observed in powder UV-Vis spectrum. Therefore, complex with small crystal field splitting in high spin, may have *d-d* transition at higher wavelength merged with the broad band at 414 nm in the powder spectrum [38].

A square planar Cu(II) complex exhibits three main *d-d* transitions ($^2B_{1g} \rightarrow {}^2A_{1g}$, $^2B_{1g} \rightarrow {}^2B_{2g}$ and $^2B_{1g} \rightarrow {}^2E_g$). The broad band at 414 nm in powder UV-Vis spectra with a low molar extinction coefficient is the combination of these three transitions [16].

EPR spectroscopy: The EPR spectra of the copper(II) complex was recorded at 305 K and X-band at a microwave frequency of 9.166131 GHz. The EPR g and G values for the copper(II) complex is presented in Table-1.

The EPR spectrum of the complex showed the presence of four distinct peaks in the low field region and a significant intensity peak in the high field region. Subsequently the $g_{\parallel}$ value was calculated from the peaks at low field region and $g_{\perp}$ value was obtained from the peak at high field region in the EPR spectrum. The g-factors was determined using the following equation:

TABLE-1
EPR g AND G VALUES FOR THE COPPER(II) COMPLEX

Complexes	$g_{\perp}$	$g_{\parallel}$	G
$[Cu(L)Cl_2]$	$g_{\perp}$; 2.0669	$g_{\parallel}$; 2.3559	5.4737

$$g = \frac{h\nu\mu_o}{B_o} = 71.45 \times \frac{\nu}{B_o}$$

where $h/\mu_o = 71.45$, $h = 6.626 \times 10^{-34}$ JS; μ_o = Bohr magneton value of 9.27×10^{-24} J/T = 9.27×10^{-27} J/mT); ν is frequency and B_o is magnetic field.

The spectral data agrees with axial spectra due to Cu^{2+} nuclear spins in the complex in which both the ^{63}Cu and ^{65}Cu nuclear spins of 3/2 caused the Zeeman line splitting into four lines corresponding to magnetic spins at 3/2, 1/2, -1/2 and -3/2. The coincidence hyperfine couplings attributed to similar moments of the two isotopes and better resolution in a particular direction of molecular axis due to anisotropy in the central hyperfine splitting was featured in the spectrum of the complex. The greater hyperfine coupling along $g_{\parallel}$ region showed large splitting in $g_{\parallel}$ region and minor splitting in $g_{\perp}$ region in EPR spectrum of the Cu^{2+} complex [39]. The EPR spectrum agreed with axial anisotropic spectra of copper(II) nuclei with four peaks at the magnetic field values along the *z*-axis and a split peaks at the magnetic field corresponding to *xy*-plane [40]. The EPR spectrum is utilized for identification and characterization of paramagnetic centers in molecules. The nature of the metal ligand bonding in the coordination compound can be predicted based on $g_{\parallel}$ value. If $g_{\parallel} > 2.3$, it indicates ionic nature whereas $g_{\parallel} < 2.3$ is indicative of covalent nature of metal-ligand bonds [41]. For the complex in this study, $g_{\parallel}$ slightly greater than 2.3 and it indicates ionic character of metal ligand covalent bonds. The g tensor values can be used to predict the geometry of the complexes. If $g_{\parallel} > g_{\perp} > g_e$ (free electron = 2.0023), it indicates ground state orientation of $d_{x^2-y^2}$ orbital and axial elongation with a square planar geometry whereas the opposite trend *i.e.* $g_{\perp} > g_{\parallel} > g_e$ (free electron = 2.0023) indicates the ground state orientation of dz^2 orbital and compression of paramagnetic centre with a tetrahedral or trigonal bipyramidal geometry [42]. The observed g tensor values of $g_{\parallel} > g_{\perp} > g_e$ (free electron = 2.0023) for the complex is indicative of unpaired electrons of the Cu(II) ion in the ground state $d_{x^2-y^2}$ orbitals and this is the characteristic feature of a square planner geometry [42]. The spin orbital coupling of metal orbitals with unpaired electrons causes the shifting of g value from g_e (2.0023) and this process depends upon the degree of covalency in complex molecule [43]. The exchange interaction between the two metal ions in the solid-state complex can be confirmed based on the geometric parameter G, calculated by the relation: = $(g_{\parallel} - 2.0023)/(g_{\perp} - 2.0023)$. A negligible interaction is inferred if $G > 4$ and significant interaction is indicated by $G < 4$ [44,45].

X-ray crystallography: Single crystals of the compound (L) suitable for X-ray diffraction study was grown by slow

evaporation in ethanol. The diffraction data was collected on Bruker D8 venture diffractometer with Photon II detector at 298 K having Mo/*K*α radiation (λ = 0.71073). The data was corrected for Lorentz and polarization effects. Multi-scan absorption correction was applied. The structure was solved by direct method using ShelXT [46] and refined by full-matrix least-squares refinement techniques on F2 using ShelXL-2019/3 [46]. All the calculations were done with the help of Olex2 version 1.5 crystallographic software [47]. For molecular graphics, the program Olex2 was used. All non-hydrogen atoms were refined anisotropically. All hydrogen atoms on the carbon were fixed geometrically with U_{iso} values of 1.2, 1.2 and 1.5 times the U_{iso} values of methylene, phenylene and methyl carbon, respectively. The hydrogen of nitrogen N_1 was located from a different Fourier map. Details of the crystal data and structure refinement for L are given in Table-2 and bond lengths and angle are given in Tables 3 and 4, respectively (CCDC No. 2428036).

TABLE-2
CRYSTAL DATA AND STRUCTURE REFINEMENT FOR L

Empirical formula	$C_{17}H_{20}N_2O_4$
Formula weight	316.35
Temperature (K)	305.00
Crystal system	Orthorhombic
Space group	$P2_12_12_1$
a (Å)	5.4258(3)
b (Å)	12.4715(9)
c (Å)	23.6349(16)
α (°)	90
β (°)	90
γ (°)	90
Volume (Å^3)	1599.32(18)
Z	4
ρ_{calc} (g/cm^3)	1.314
μ (mm^{-1})	0.094
F(000)	672.0
Crystal size (mm^3)	0.39 × 0.141 × 0.102
Radiation	Mo/*K*α (λ = 0.71073)
2θ range for data collection (°)	6.534 to 51.402
Index ranges	$-6 \le h \le 6, -15 \le k \le 15, -28 \le l \le 28$
Reflections collected	33004
Independent reflections	3050 [R_{int} = 0.0822, R_{sigma} = 0.0373]
Data/restraints/parameters	3050/0/212
Goodness-of-fit on F^2	1.118
Final R indexes [I ≥ 2σ(I)]	R_1 = 0.0479, wR_2 = 0.0959
Final R indexes [all data]	R_1 = 0.0622, wR_2 = 0.1013
Largest diff. peak/hole (e Å^{-3})	0.14/-0.12
Flack parameter	0.2(7)

The structure of the Schiff base L together with the atom labeling scheme is shown in Fig. 1. The compound crystallizes in a non-centrosymmetric $P2_12_12_1$ orthorhombic space group with one molecule in the asymmetric unit. The pyrone ring of the coumarin moiety has deprotonated phenolic oxygen O_3 (C_8-O_3 = 1.253 Å) and nitrogen N_1 is protonated, which indicated the existence of zwitter ionic form in the crystalline solid. The bond length C_1-O_1 (1.213 Å) indicates the double bond character which in turn explains the existence of the pyrone ring of the coumarin moiety in the crystal structure of the compound. The

TABLE-3
BOND LENGTHS FOR L

Atom	Atom	Length (Å)	Atom	Atom	Length (Å)
C1	C9	1.445(4)	C9	C10	1.433(4)
C1	O1	1.213(4)	C10	C11	1.497(4)
C1	O2	1.386(4)	C10	N1	1.304(4)
C2	C3	1.386(4)	C12	C13	1.511(4)
C2	C7	1.377(4)	C12	N1	1.460(4)
C2	O2	1.375(4)	C13	N2	1.456(4)
C3	C4	1.370(5)	C14	C15	1.503(5)
C4	C5	1.386(5)	C14	N2	1.461(4)
C5	C6	1.368(4)	C15	O4	1.420(4)
C6	C7	1.395(4)	C16	C17	1.503(5)
C7	C8	1.467(4)	C16	O4	1.411(4)
C8	C9	1.447(4)	C17	N2	1.464(4)
C8	O3	1.253(3)			

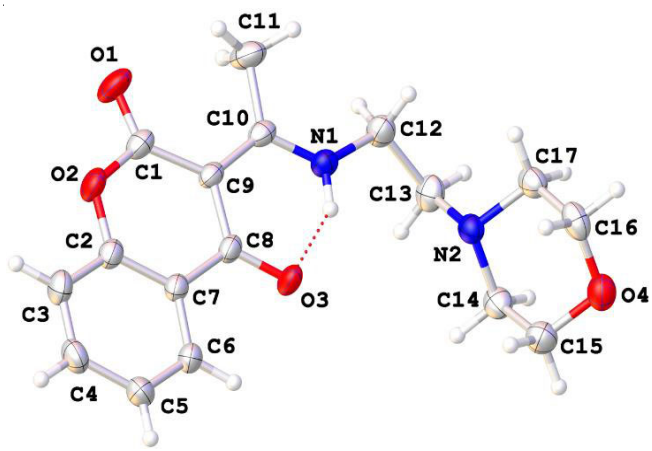

Fig. 1. ORTEP diagram of L drawn in 30% thermal probability ellipsoids showing atomic numbering scheme

bond angles around the C_8 *i.e.* (O_3-C_8-C_9) = 123.5°, (O3-C_8-C_7) = 119.2°, (C_7-C_8-C_9) = 117.3° and that around the C_1 *i.e.* (O_2-C_1-O_1) = 113.4°, (O_2-C_1-C_9) = 118.4°, (O_1-C_1-O_9) = 128.2° also indicate aromatic hydrocarbon (sp^2 hybridization) in the C8 and C1 carbon. The bond length C_8-C_9 (1.447 Å), C_9-C_{10} (1.433 Å) and C_{10}-N_1 (1.304 Å) lie intermediate between single and double bond lengths of π-electron from deprotonated phenolic group to the imine group of the coumarin Schiff base L. This is also supported by the bond angle around C_{10} *i.e.* (C_9-C_{10}-C_{11}) = 123.2°, (C_{11}-C_{10}-N_1) = 116.8°, (C_9-C_{10}-N_1) = 119.9° and that around N1 *i.e.* (C_{10}-N_1-C12) = 127.3°, (C_{10}-N_1-$N_{(1)}$H) = 112° and (C_{12}-N_1-$N_{(1)}$H) = 120°, which indicated aliphatic hydrocarbon (sp^3 hybridization) in C_{10} and N_1 atoms. C_{12} and C_{13} have distorted tetrahedral bond angle of 108.9° and 113.4° indicating their usual SP^3 hybridization of single bond in between N_1-C_{12},C_{12}-C_{13} and C_{13}-N_2 in the crystal structure of ligand, L [48].

The only acidic hydrogen (H1) involved in intramolecular hydrogen bonding with O3 (N1–H1···O3 = 1.78(3) Å). The molecule attracting with the neighbouring molecules *via* C–H···O intermolecular hydrogen bonding interactions. Fig. 2 shows the different kinds of C–H···O interactions present in the molecule. These are summarized in Table-5.

Pharmacokinetics analysis: The path from lead to clinical therapeutic candidate is the difficult issue in drug research and

TABLE-4
BOND ANGLES FOR L

Atom	Atom	Atom	Angle (°)	Atom	Atom	Atom	Angle (°)
O1	C1	C9	128.2(3)	C10	C9	C1	120.0(3)
O1	C1	O2	113.4(3)	C10	C9	C8	120.0(2)
O2	C1	C9	118.4(3)	C9	C10	C11	123.2(3)
C7	C2	C3	121.5(3)	N1	C10	C9	119.9(3)
O2	C2	C3	117.0(3)	N1	C10	C11	116.8(3)
O2	C2	C7	121.5(3)	N1	C12	C13	108.9(3)
C4	C3	C2	119.2(3)	N2	C13	C12	113.4(3)
C3	C4	C5	120.4(3)	N2	C14	C15	110.3(3)
C6	C5	C4	119.9(3)	O4	C15	C14	112.1(3)
C5	C6	C7	120.8(3)	O4	C16	C17	112.2(3)
C2	C7	C6	118.2(3)	N2	C17	C16	110.9(3)
C2	C7	C8	119.9(3)	C10	N1	C12	127.3(3)
C6	C7	C8	121.9(3)	C13	N2	C14	111.1(2)
C9	C8	C7	117.3(2)	C13	N2	C17	111.6(3)
O3	C8	C7	119.2(3)	C14	N2	C17	108.8(2)
O3	C8	C9	123.5(3)	C2	O2	C1	122.8(2)
C1	C9	C8	120.0(3)	C16	O4	C15	108.8(3)

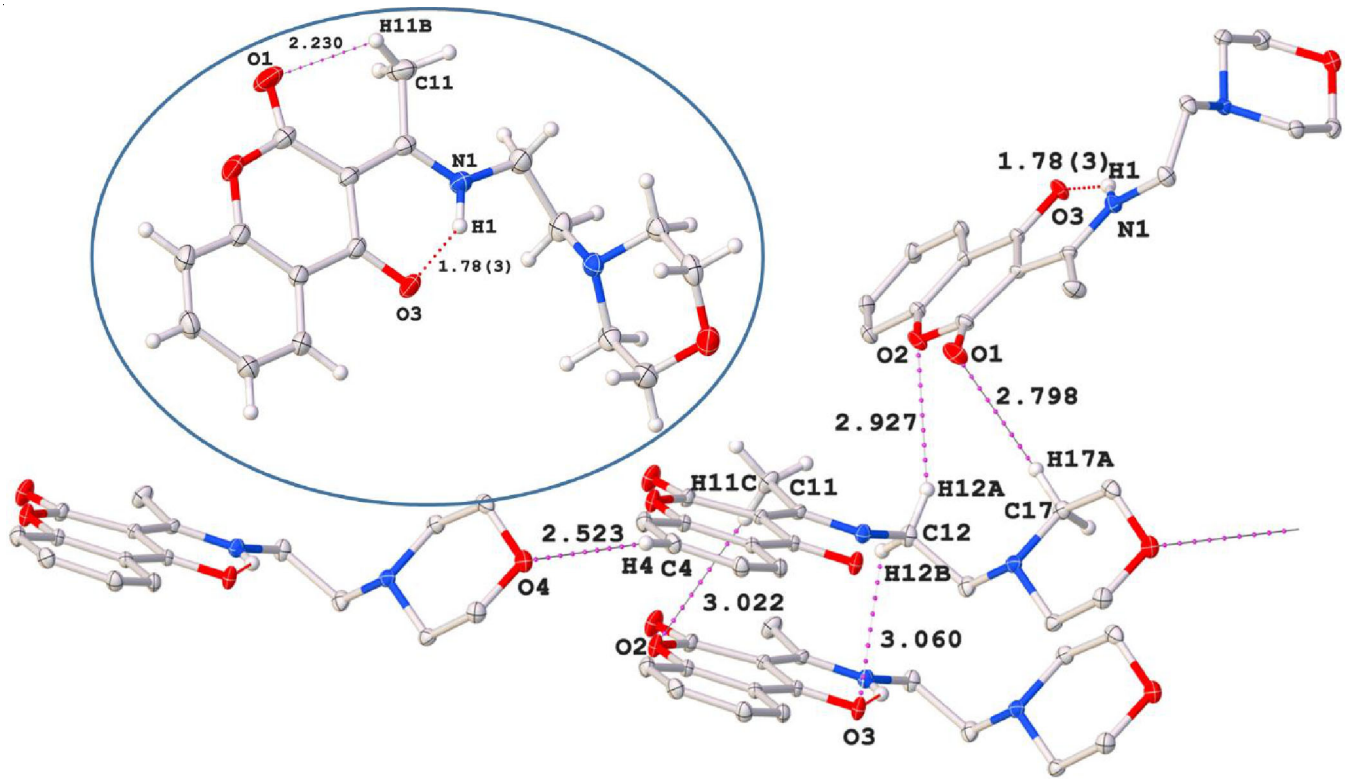

Fig. 2. Diagram showing the intermolecular hydrogen bonding in the molecule. Intramolecular hydrogen bonding is shown in circle

TABLE-5
NON-COVALENT INTERACTIONS PRESENT IN THE CRYSTAL STRUCTURE

D	H	A	d(D-H) (Å)	d(H-A) (Å)	d(D-A) (Å)	D-H-A (°)
Intramolecular hydrogen bonds						
C11	H11B	O1	0.96	2.230(3)	2.770(5)	114.6
N1	H1	O3	0.90(3)	1.78(3)	2.568(3)	145(3)
Intermolecular hydrogen bonds						
C4	H4	O4[1]	0.930	2.523(2)	3.305(4)	141.9(2)
C17	H17A	O1[2]	0.970	2.798(3)	3.657(5)	148.0(2)
C11	H11C	O2[3]	0.960	3.022(2)	3.926(5)	157.7(2)
C12	H12A	O2[4]	0.970	2.927(2)	3.827(4)	154.6(2)
C12	H12B	O3[5]	0.970	3.060(3)	3.579(5)	115.0(2)

-1+x, 1+y, +z, 2. 1-x, -1/2+y, 3/2-z, 3. 1+x, +y, +z, 4. 1-x, -1/2+y, 3/2-z, 5. 1+x, +y, +z

TABLE-6
ADMET PROFILE

ADMET parameters	L	[$CuLCl_2$]	Ref. (PF-06459988)
Water solubility (log mol/L)	-2.741	-4.359	-3.028
Caco-2 permeability (log Papp in 10^{-6} cm/s)	0.511	1.115	0.292
Intestinal absorption (% absorbed)	96.12	90.65	74.607
VDss (log L/kg)	0.766	0.574	0.99
BBB permeability (log BB)	-0.314	0.504	-1.549
CNS permeability (log PS)	-2.931	-2.979	-3.174
CYP1A2 inhibitor	No	No	No
CYP2C19 inhibitor	No	No	No
CYP2C9 inhibitor	No	No	No
CYP2D6 inhibitor	No	No	No
CYP3A4 inhibitor	No	No	No
Total clearance (log mL/min)	0.783	1.201	0.907
Ames toxicity	Yes	No	No
Hepatotoxicity	Yes	Yes	Yes
Toxicity class	IV	IV	III

development. In order for a drug to be taken into consider- it needs to be very selective, have few side effects and have enough biodistribution and bioavailability to cause the intended reaction in the body [49]. Drug candidates often have a high rate of withdrawal during final stages of the research, mostly due to their effectiveness and the inevitable occurrence of side effects, which are primarily caused by ADMET issues [50]. Before investing in costly clinical trials, pharmaceutical companies mostly rely on *in silico* ADME-Tox prediction to select the drug candidate. The pkCSM tool helps assess the potency, pharmacological properties (Table-6) and related safety concerns of pharmaceuticals [51]. The synthesized Schiff base ligand (L) and complex, [$CuLCl_2$] showed significant human intestinal absorption (HIA) 96.2 and 90.65%, respectively. The permeability of the colon cancer cell line (Caco-2) is measured in order to evaluate the absorption and bioavailability of oral drugs; an apparent permeability coefficient (Papp) value > 8×10^{-6} cm/s is defined as satisfactory permeability value. The blood-brain barrier (BBB) partially crossed by ligands with a log BB ≤ 0.3 are poorly distributed to the brain. To avoid neurotoxicity, it is preferable for drugs whose action site is unrelated to brain to not cross the BBB [52]. Cytochrome P450 (CYPs) enzymes are crucial for detoxification and metabolism of drugs and both ligand and [$CuLCl_2$] do not inhibit CYPs, which is an indication of a healthy metabolism. Topological polar surface area (TPSA) is a guideline to assess the capacity of a drug to permeate cells: TPSA > 140 $Å^2$ denotes poor permeability of drugs, while TPSA ≤ 60 $Å^2$ denotes high permeability [53]. The Lipinski's rule of five was not violated indicating drug-like qualities (Table-7). The ProTox-3.0 server is helpful for analyzing the toxicities under which, toxicity classes have been grouped into six broad groups, with reference ligand, indicating that Schiff base ligand and [$CuLCl_2$] is comparatively less toxic [25].

The primary indicators used to analyze the docking outcome are the binding energy, the number of hydrogen bonds and the interacting amino acids. The molecular docking investigation showed preferred binding interactions of ligand with active pockets of EGFR compared with the reference ligand (PF-06459988), a novel third generation inhibitor of EGFR T790M mutants [54]. Hydrogen bonds are important in the recognition of protein-ligand interactions and play a vital role in selecting appropriate binding affinity and stabilization of protein-ligand complexes. The greater stability of its complex is indicated by its low binding energy. In the study of Schiff base ligand and [$CuLCl_2$], docked with EGFR protein, both interacted with the catalytic residues. The Schiff base ligand has an adequate alignment with the binding pocket of EGFR which is comparable to the reference ligand, based on their docking scores and interacting residues. Schiff base ligand shows the acceptable binding energy of -7.3 kcal/mol and accompanied H-bond interactions with catalytic residue: Cys 797 (Fig. 3). More interestingly, the complex [$CuLCl_2$], accompanied significant binding affinity of -8.0 kcal/mol in the binding site of target protein, which predicts the suitability of Schiff base ligand and [$CuLCl_2$] potency towards the anticancer activity.

TABLE-7
DRUG-LIKE PROPERTIES

Parameters	L	[$Cu(L)Cl_2$]	Ref. (PF-06459988)
Molecular weight (g/mol)	316.35	452.83	431.88
No. of H-bond acceptors (HBA)	6	6	6
No. of H-bond donors (HBD)	1	1	2
Log P	2.67	3.01	2.88
TPSA ($Å^2$)	75.27		110.19

Conclusion

Single crystal X-ray diffraction study revealed the structure of coumarin aminoethyl morpholine Schiff base. The anticancer activity against MCF-7 showed IC_{50}; 256.60 ± 0.11 and IC_{50}; 118.50 ± 0.40 for the Schiff base ligand and complex, respectively. Comparatively, complex was much potent than the Schiff base ligand in cytotoxicity. The molecular docking result manifests that the Schiff base ligand (L) and its copper complex, [$CuLCl_2$] achieved significant binding interactions *via* H-bonds with catalytic residue Cys 797 with binding energy of -7.3 kcal/mol and -8.0 kcal/mol, respectively, which is comparable with the reference drug. The cell cycle analysis of the complex, showed a lower proportion of cells in G2 phase. Thus, the overall findings of the study show that these compounds have anticancer potency which needed further study.

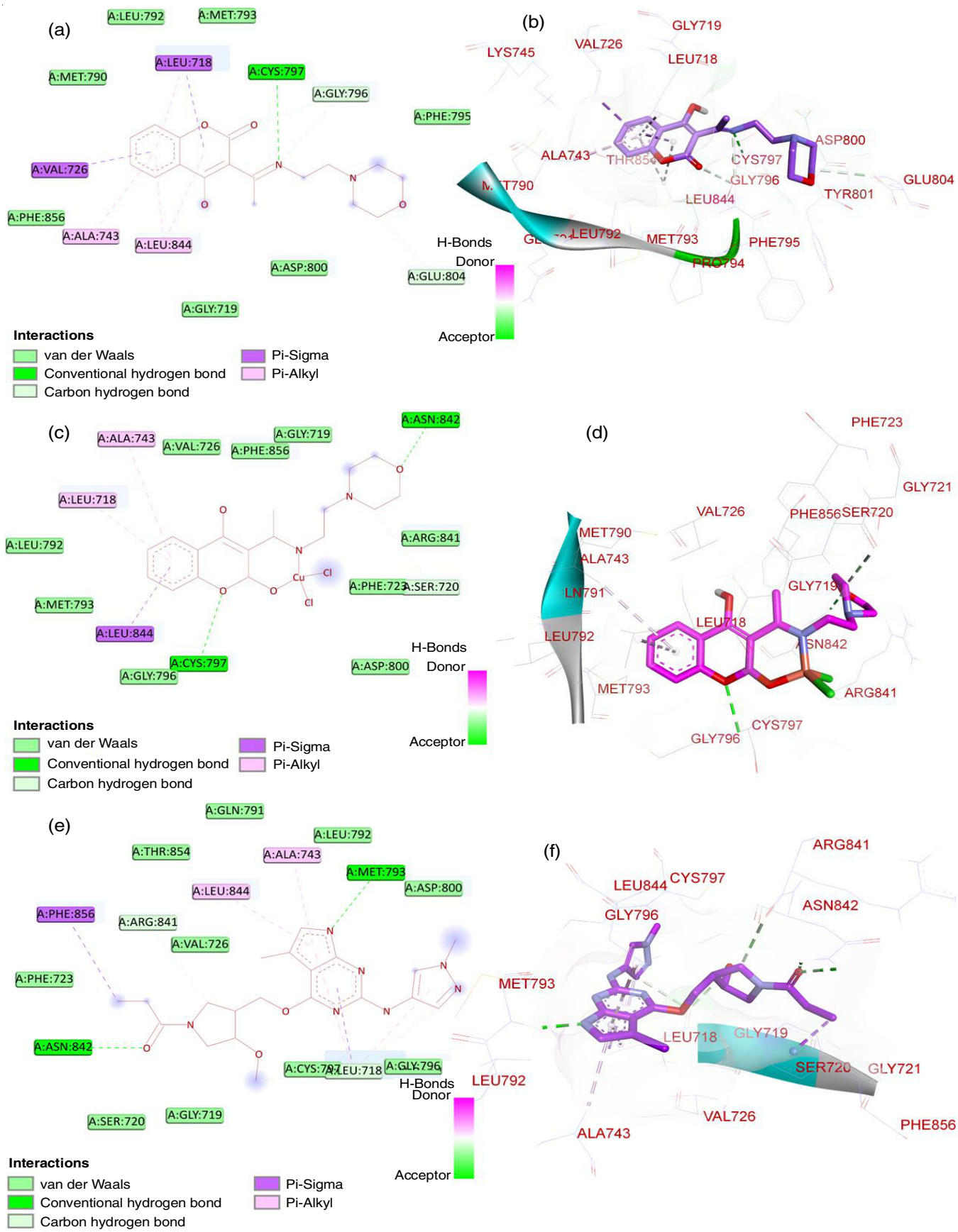

Fig. 3. (a) and (b) 2D and 3D structures of 4-hydroxy-3-{(1*E*)-N-[2-(morpholin-4-yl)ethyl]ethanimidoyl}-2*H*-1-benzopyran-2-one (L) complexed with EGFR protein; (c) and (d) 2D and 3D structures of $[CuLCl_2]$ complexed with EGFR protein; and (e) and (f) 2D and 3D structures of reference ligand (PF-06459988) complexed with EGFR protein

ACKNOWLEDGEMENTS

The authors sincerely acknowledge Indian Institute of Technology Madras, for EPR data, CHN analysis, HRMS spectra, XRD data and Indian Institute of Science, Bangalore, India for NMR spectrum. The authors also acknowledge Nepal Academy of Science and Technology, Lalitpur, Nepal for UV-Vis and FT-IR data and the Department of Applied Science and Chemical Engineering, Institute of Engineering, Tribhuvan University, Kathmandu, Nepal for solid-state UV-Vis spectra. Aakaar Biotechnologies Pvt. Ltd. Lucknow, India is also acknowledged for the anticancer screening.

CONFLICT OF INTEREST

The authors declare that there is no conflict of interests regarding the publication of this article.

REFERENCES

1. A. Rawat and A.V.B. Reddy, *Eur. J. Med. Chem. Rep.*, **5**, 100038 (2022); https://doi.org/10.1016/j.ejmcr.2022.100038
2. R.L. Siegel, A.N. Giaquinto and A. Jemal, *CA Cancer J. Clin.*, **74**, 12 (2024); https://doi.org/10.3322/caac.21820
3. N.S. Abdel-Kader, H. Moustafa, A.L. El-Ansary, O.E. Sherif and A.M. Farghaly, *New J. Chem.*, **45**, 7714 (2021); https://doi.org/10.1039/D0NJ05688J
4. Q.H. Cui, W.B. Li, Z.Y. Wang, K.Y. Xu, S. Wang, J.T. Shi, L.W. Zhang and S.W. Chen, *Bioorg. Chem.*, **128**, 106117 (2022); https://doi.org/10.1016/j.bioorg.2022.106117
5. K.M. Amin, A.M. Taha, R.F. George, N.M. Mohamed and F.F. Elsenduny, *Arch. Pharm.*, **351**, 1700199 (2018); https://doi.org/10.1002/ardp.201700199
6. M.K. Gupta, S. Kumar and S. Chaudhary, *Asian J. Pharm. Clin. Res.*, **12**, 27 (2019); https://doi.org/10.22159/ajpcr.2019.v12i3.30635
7. F. Annunziata, C. Pinna, S. Dallavalle, L. Tamborini and A. Pinto, *Int. J. Mol. Sci.*, **21**, 4618 (2020); https://doi.org/10.3390/ijms21134618
8. A.K. Yadav, R.M. Shrestha and P.N. Yadav, *Eur. J. Med. Chem.*, **267**, 116179 (2024); https://doi.org/10.1016/j.ejmech.2024.116179
9. M.A. Musa, J.S. Cooperwood and M.O.F. Khan, *Curr. Med. Chem.*, **15**, 2664 (2008); https://doi.org/10.2174/092986708786242877
10. Y. Tang, Y. Li, J. Han, Y. Mao, L. Ni and Y. Wang, *Spectrochim. Acta A Mol. Biomol. Spectrosc.*, **208**, 299 (2019); https://doi.org/10.1016/j.saa.2018.10.019
11. M.N. Uddin, S.S. Ahmed and S.M.R. Alam, *J. Coord. Chem.*, **73**, 3109 (2020); https://doi.org/10.1080/00958972.2020.1854745
12. H.S. Adhikari, A. Garai and P.N. Yadav, *Carbohydr. Res.*, **526**, 108796 (2023); https://doi.org/10.1016/j.carres.2023.108796
13. N.K. Singh, S. Sharma, A. Krishnakumar, R.K. Choudhary, A.A. Kumbhar, R.J. Butcher, Y.R. Pokharel and P.N. Yadav, *Inorg. Chem. Commun.*, **143**, 109767 (2022); https://doi.org/10.1016/j.inoche.2022.109767
14. H.S. Adhikari, A. Garai, K.D. Manandhar and P.N. Yadav, *ACS Omega*, **7**, 30978 (2022); https://doi.org/10.1021/acsomega.2c02966
15. J.E. Summerton, *Curr. Top. Med. Chem.*, **7**, 651 (2007); https://doi.org/10.2174/156802607780487740
16. N.S. Gwaram and P. Hassandarvish, *J. Appl. Pharm. Sci.*, **4**, 75 (2014); https://doi.org/10.7324/JAPS.2014.401014
17. M.R. Bhatta, S. Adhikari, J. Lamichhane and P.N. Yadav, *J. Nepal Chem. Soc.*, **31**, 43 (2013).
18. H.R. Eisenhauer and K.P. Link, *J. Am. Chem. Soc.*, **75**, 2044 (1953); https://doi.org/10.1021/ja01105a006
19. J.V. Meerloo, G.J.L. Kaspers and J. Cloos, *Methods Mol. Biol.*,, **731**, 237 (2011); https://doi.org/10.1007/978-1-61779-080-5_20
20. D.B.M. Tihãuan, L.M. Berca, M. Adascalului, A.M. Sanmartin, S. Nica and D. Cimponeriu, *Rom. Biotechnol. Lett.*, **25**, 1832 (2020); https://doi.org/10.25083/rbl/25.4/1832.1842
21. F. Khan, F. Ahmed, P.N. Pushparaj, A. Abuzenadah, T. Kumosani, E. Barbour, M. AlQahtani and K. Gauthaman, *PLoS One*, **11**, 10 (2016); https://doi.org/10.1371/journal.pone.0158963
22. A.K. Yadav, N. Singh, M. Silwal, A. Adhikari and P.N. Yadav, *Results Chem.*, **11**, 101794 (2024); https://doi.org/10.1016/j.rechem.2024.101794
23. N.S. Gwaram, *ChemSearch J.*, **8**, 56 (2017).
24. A. Daina, O. Michielin and V. Zoete, *Sci. Rep.*, **7**, 42717 (2017); https://doi.org/10.1038/srep42717
25. P. Banerjee, A.O. Eckert, A.K. Schrey and R. Preissner, *Nucleic Acids Res.*, **46(W1)**, W257 (2018); https://doi.org/10.1093/nar/gky318
26. D.E.V. Pires, T.L. Blundell and D.B. Ascher, *J. Med. Chem.*, **58**, 4066 (2015); https://doi.org/10.1021/acs.jmedchem.5b00104
27. H. Cheng, S.K. Nair, B.W. Murray, C. Almaden, S. Bailey, S. Baxi, D. Behenna, S. Cho-Schultz, D. Dalvie, D.M. Dinh, M.P. Edwards, J.L. Feng, R.A. Ferre, K.S. Gajiwala, M.D. Hemkens, A. Jackson-Fisher, M. Jalaie, T.O. Johnson, R.S. Kania, S. Kephart, J. Lafontaine, B. Lunney, K.K.-C. Liu, Z. Liu, J. Matthews, A. Nagata, S. Niessen, M.A. Ornelas, S.T. M. Orr, M. Pairish, S. Planken, S. Ren, D. Richter, K. Ryan, N. Sach, H. Shen, T. Smeal, J. Solowiej, S. Sutton, K. Tran, E. Tseng, W. Vernier, M. Walls, S. Wang, S.L. Weinrich, S. Xin, H. Xu, M.-J. Yin, M. Zientek, R. Zhou and J.C. Kath, *J. Med. Chem.*, **59**, 2005 (2016); https://doi.org/10.1021/acs.jmedchem.5b01633
28. G.M. Morris, R. Huey, W. Lindstrom, M.F. Sanner, R.K. Belew, D.S. Goodsell and A.J. Olson, *J. Comput. Chem.*, **30**, 2785 (2009); https://doi.org/10.1002/jcc.21256
29. A.M. Ahmed, Q.R. Ibrahim and A.K.T. Mohammad, *Bas. J. Sci.*, **40**, 43 (2022); https://doi.org/10.29072/basjs.20220103
30. N. Raman, J. Joseph, A. Sakthivel and R. Jeyamurugan, *J. Chil. Chem. Soc.*, **54**, 354 (2009); https://doi.org/10.4067/S0717-97072009000400006
31. R.M. Shrestha, K. Mahiya, A. Shrestha, S.R. Mohanty, S.K. Yadav and P.N. Yadav, *Inorg. Chem. Commun.*, **161**, 112142 (2024); https://doi.org/10.1016/j.inoche.2024.112142
32. N.K. Singh, S. Shrestha, N. Shahi, R.K. Choudhary, A.A. Kumbhar, Y.R. Pokharel and P.N. Yadav, *Rasayan J. Chem.*, **14**, 1600 (2021); https://doi.org/10.31788/RJC.2021.1436341
33. V. Arjunan, S. Sakiladevi, M.K. Marchewka and S. Mohan, *Spectrochim. Acta A Mol. Biomol. Spectrosc.*, **109**, 79 (2013); https://doi.org/10.1016/j.saa.2013.01.100
34. M.M. Abdou, *Arab. J. Chem.*, **10**, S3664 (2017); https://doi.org/10.1016/j.arabjc.2014.04.005
35. R.M. Shrestha, K. Mahiya, A. Shrestha, S.R. Mohanty, S.K. Yadav and P.N. Yadav, *J. Mol. Struct.*, **1299**, 136945 (2024); https://doi.org/10.1016/j.molstruc.2023.136945
36. S. Indira, R. Anbarasan, B.S. Sreeja, M. Srinivasan and P. Manikandan, *Research Square*, 1-19 (2022); https://doi.org/10.21203/rs.3.rs-1513188/v1
37. B.S. Creaven, B. Duff, D.A. Egan, K. Kavanagh, G. Rosair, V.R. Thangella and M. Walsh, *Inorg. Chim. Acta*, **363**, 4048 (2010); https://doi.org/10.1016/j.ica.2010.08.009
38. B.S. Creaven, M. Devereux, D. Karcz, A. Kellett, M. McCann, A. Noble and M. Walsh, *J. Inorg. Biochem.*, **103**, 1196 (2009); https://doi.org/10.1016/j.jinorgbio.2009.05.017
39. J. Peisach and W.E. Blumberg, *Arch. Biochem. Biophys.*, **165**, 691 (1974); https://doi.org/10.1016/0003-9861(74)90298-7
40. C. Drouza, S. Spanou and A.D. Keramidas, *Intech Open Topic From EPR Res.*, 45 (2019); https://doi.org/10.5772/intechopen.79844

41. R.C. Chikate, A.R. Belapure, S.B. Padhye and D.X. West, *Polyhedron*, **24**, 889 (2005); https://doi.org/10.1016/j.poly.2005.02.011
42. E. Garribba and G. Micera, *J. Chem. Educ.*, **83**, 1229 (2006); https://doi.org/10.1021/ed083p1229
43. A. Ahmed and R.A. Lal, *Arab. J. Chem.*, **10**, S901 (2017); https://doi.org/10.1016/j.arabjc.2012.12.026
44. B.J. Hathaway and D.E. Billing, *Coord. Chem. Rev.*, **5**, 143 (1970); https://doi.org/10.1016/S0010-8545(00)80135-6
45. P.F. Rapheal, E. Manoj and M.R.P. Kurup, *Polyhedron*, **26**, 818 (2007); https://doi.org/10.1016/j.poly.2006.09.091
46. G.M. Sheldrick, *Acta Crystallogr. A Found. Adv.*, **71**, 3 (2015); https://doi.org/10.1107/S2053273314026370
47. O.V. Dolomanov, L.J. Bourhis, R.J. Gildea, J.A.K. Howard and H. Puschmann, *J. Appl. Cryst.*, **42**, 339 (2009); https://doi.org/10.1107/S0021889808042726
48. H.V.P. Hollauer, R.C. Vilas Novas, G.P. Guedes, C.D. Buarque and L.B.L. Escobar, *Acta Crystallogr. E Crystallogr. Commun.*, **79**, 842 (2023); https://doi.org/10.1107/S2056989023007351
49. F.F. Hefti, *BMC Neurosci.*, **9(S3)**, 1 (2008); https://doi.org/10.1186/1471-2202-9-S3-S7
50. S.M. Paul, D.S. Mytelka, C.T. Dunwiddie, C.C. Persinger, B.H. Munos, S.R. Lindborg and A.L. Schacht, *Nat. Rev. Drug Discov.*, **9**, 203 (2010); https://doi.org/10.1038/nrd3078
51. M. Muehlbacher, G.M. Spitzer, K.R. Liedl and J. Kornhuber, *J. Comput. Aided Mol. Des.*, **25**, 1095 (2011); https://doi.org/10.1007/s10822-011-9478-1
52. J. Fernandes and C.R. Gattass, *J. Med. Chem.*, **52**, 1214 (2009); https://doi.org/10.1021/jm801389m
53. H. Van de Waterbeemd, *In Silico* Models to Predict Oral Absorption, In: Comprehensive Medicinal Chemistry II, **5**. pp. 669-697 (2007); https://doi.org/10.1016/B0-08-045044-X/00145-0
54. M. Dinic, U. Pecikoza, J. Djokic, R. Stepanovic-Petrovic, M. Milenkovic, M. Stevanovic, N. Filipovic, J. Begovic, N. Golic and J. Lukic, *Front. Pharmacol.*, **9**, 1 (2018); https://doi.org/10.3389/fphar.2018.00001